JOURNAL OF PROPULSION AND POWER
Vol. 22, No. 5, September–October 2006

Study of Plasma-Propellant Interaction During Normal Impingement

Jianquan Li,* Thomas A. Litzinger,† Malay Das,‡ and Stefan T. Thynell†
Pennsylvania State University, University Park, Pennsylvania 16802

DOI: 10.2514/1.17286

This paper describes an effort to investigate the transient process of an electrothermal plasma normally impinging on a plate or a solid propellant. The objective of this effort was to develop a better understanding of the fundamental aspects of this process to facilitate the development of the plasma ignition system for use in electrothermal chemical propulsion applications. The plasma is produced through an electrical discharge occurring within a polyethylene capillary. The high-temperature and high-pressure plasma exited from the capillary into an ambient air environment and impinged normally onto a plate. Pressure transducers mounted on the plate were used to obtain the stagnation pressure of the plasma jet, and a multiple CCD imaging system was used to visualize this highly transient process. Tests were also performed with the stagnation plate replaced by a solid propellant sample. Plasma-induced surface changes were examined using a scanning electron microscope, mass loss of the propellant was measured, and decomposition species were analyzed using a triple quadrupole mass spectrometer. The results show that when the distance between the capillary exit port and the plate was varied, changes in plasma jet structure, stagnation pressures, and mass losses of the propellant were significant.

Nomenclature

i_1	=	electric current flowing through the capillary plasma
i_2	=	electric current flowing parallel to the capillary plasma
$L_{\text{n-p}}$	=	distance between nozzle exit to stagnation plate
$L_{\text{n-s}}$	=	distance between nozzle exit to propellant sample
p	=	pressure
t	=	time

Introduction

THE concept of electrothermal-chemical (ETC) propulsion has been studied for a number of years. This concept introduces electrical energy in the form of an electrothermal (ET) plasma produced through exploding a metallic wire and sustained by the ablation of surrounding capillary wall material of either the propellant [1] or an inert polymer [2–5]. Results from laboratory experiments and actual firing tests have clearly indicated that ETC plasma ignition can offer several attractive benefits over conventional chemical powder ignition, including precision ignition in terms of shorter and more reproducible ignition delay [6], mitigation of gun performance sensitivity to ambient temperature [7], and the ability to reliably ignite low-vulnerability ammunition (LOVA) propellants [8] and high-loading density propellant charges [9,10]. However, optimization of the ETC igniter design relies on a clear and complete understanding of the underlying fundamentals that account for these observed benefits.

Over the years, substantial research activities have been conducted on the subject of plasma-propellant interaction (PPI), and through these research efforts several hypotheses have been proposed to describe the processes during PPI. One of these hypotheses is that radiant heat flux from the plasma to the propellant can lead to in-depth heating of the propellant so that it burns at higher temperatures with an enhanced burn rate [11–14]; another hypothesis is that plasma species can augment the chemical kinetics at or near the propellant surface; a third one is that the mechanical impact, which may produce increased surface area of the propellant through fracture, is important [15]; and the fourth is that metallic vapor deposition can be an important heat transfer mechanism in the ignition phase [16,17].

The work presented in this paper investigated the effect of the separation distance of a sample from the plasma exit on the response of JA2 propellant at fixed plasma energy and sought to find evidence of the different mechanisms thought to play a role in plasma ignition. The effect of separation on the pressure field imposed on the sample was investigated, and the results were used to estimate the mechanical forces exerted on the sample. The variation of the jet structure with distance was also observed. Recovered samples were subjected to scanning electron microscopy to observe changes in surface structure that are attributable to radiation and to check for the presence of metal particles on the surface; x-ray detection was also used to observe changes in elemental composition and the presence of metals. Finally, mass spectrometry was used to detect the presence of reaction products from the propellant during an ignition event.

Experimental

The overall experimental setup and diagnostic methods are schematically shown in Fig. 1. The plasma is produced through a capillary discharge in the plasma generator. The main diagnostics involved the use of an ultra high-speed CCD camera, silicon diodes, Kistler pressure transducers as well as a triple quadrupole mass spectrometer (not shown in the figure). A more detailed description of the setup can be found elsewhere [18,19] and hence a summary is given herein.

The plasma generator is driven by a resistance-inductance-capacitor based electrical circuit, which mainly comprises an energy storage component that consists of high-voltage fast-discharge capacitors with a total capacitance of 192 μF, pulse-shaping components including a 20 μH inductor and a crowbar diode, and a floating high-voltage mercury switch (ignitron) as the trigger unit. The capacitors can be charged up to 10 kV corresponding to a maximum energy of 9.6 kJ. The plasma chamber consists of a capillary liner, a fine metallic wire, electrodes, and other conducting or nonconducting housing hardware. The capillary liner, made of

Received 27 April 2005; revision received 21 April 2005; accepted for publication 27 January 2006.

*Postdoctoral Scholar, Department of Mechanical and Nuclear Engineering. Member AIAA.
†Professor, Department of Mechanical and Nuclear Engineering. Senior Member AIAA.
‡Research Assistant, Department of Mechanical and Nuclear Engineering. Member AIAA.

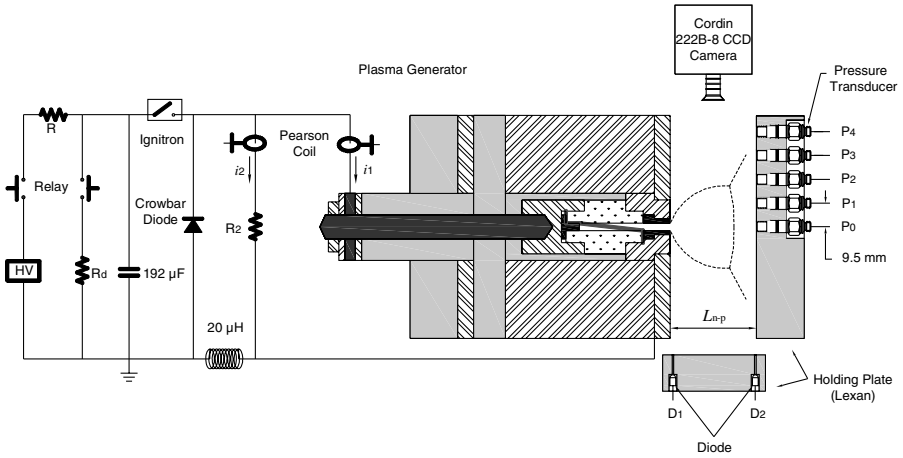

Fig. 1 Overall experimental setup.

high-density polyethylene (PE, $[C_2H_4]_n$), has a length of 26 mm and a typical diameter of 3.2 mm. Two electrodes made of copper-tungsten alloy (30% Cu, 70% W) are located at each end of the capillary and connected by a 40 AWG copper filament (0.08 mm in diameter), which serves as the discharge initiator. After being formed immediately upon triggering the ignitron, the plasma flows through a nozzle (cathode) into the open air. The nozzle has dimensions of 3.2 mm (orifice diameter) and 13 mm (length). During an experiment, two current transducers (Pearson coils) were used to measure the instantaneous currents of i_1 and i_2. The voltage across the plasma can then be deduced from i_2 and the resistance of R_2, which is connected in parallel with the flow of i_1.

Two Lexan plates were used to hold other diagnostics. One is placed laterally and the other vertically. Two silicon diodes mounted on the lateral plate were used to determine plasma emergence from the exit port (left diode) and plasma arrival at the vertical plate (right diode). The left diode (D_1) is located directly below the plasma exit port, and the right diode (D_2) is also located below the plasma flow, but is placed at a distance of $L_{n\text{-}p}$ from D_1. Both diodes thus have a side view of the plasma flow. To have a better spatial resolution, only emission of the plasma that passes through a long (10 mm) and small hole (0.71 mm in diameter) is allowed to reach the diode, and emission from all other directions is blocked by using black tape to cover the holding plate. The incident power on the diodes is thus reduced significantly. The diodes cover a spectral range of 300–900 nm and have a response time < 10 ns.

The vertical plate was equipped with either pressure transducers for stagnation pressure measurements or a sample holder for the propellant samples (not shown in Fig. 1). Temporal variations in the local stagnation pressure were recorded at five locations (9.5 mm apart) along the plate. Two models of Kistler pressure transducers, one (211B3) having a measuring range of 0–500 psig and the other (211B1) of 0–10,000 psig, were used in the experiment to accommodate varying test conditions. A thin layer of electrical insulation tape was used to prevent the transducers' sensing surfaces from being directly exposed to the charged particles in the plasma.

Plasma jet emission images (side view) were taken using an intensified, multiple charge coupled device (CCD) imaging system, Cordin 222-B, which consists of 8 CCDs and is capable of acquiring 16 images, each with a pixel resolution of 1,300 by 1,030, a 10-bit dynamic range, and exposure gates down to 10 ns. The first eight images can be acquired at a speed of up to 10^8 images per second, followed by a delay of approximately 1 μs, and then a second set of eight images at the same rate is acquired.

Surface morphology of plasma-exposed propellant samples was imaged by a FEI-Philips XL-20 scanning electron microscope (SEM), which is equipped with an energy dispersive spectrometer (EDS). The characteristic x rays produced during the scanning electron microscopy of the samples were detected by EDS to identify the elemental compositions of the sample surface areas of interest. The EDS has a spatial resolution of a few cubic micrometers.

The mass losses of propellant samples were obtained by weighing the sample right before and within a few minutes after a test using a microscale. To determine the consistency, at least two tests under the same conditions were performed, and average mass loss values are reported.

Decomposition products of the propellant during plasma impingement were sampled by a microprobe and identified by an Extrel triple quadrupole mass spectrometer (TQMS) equipped with a Merlin Automation control system. Differentiation of species at the same mass-to-charge ratio was realized by a MS/MS method through running the TQMS in "daughter mode." A detailed description of the TQMS system can be found in [20,21].

A Nicolet 120/150 MultiPro data acquisition system along with its ProView software was used for pressure and current measurements. Data acquisition was performed at 1 MHz using 12-bit transient recorders with a minimum bandwidth of 400 kHz.

Results and Discussion

Capillary Discharge Pulse

Formation of the capillary plasma is initiated by exploding the copper wire and sustained by ablating the capillary wall material as a result of intense heat transfer from the initial plasma to the capillary wall. This process is monitored by measuring electric currents that flow through the plasma (i_1) and through the bypass resistor R_2 (i_2). Unless otherwise mentioned, all tests in this work were conducted at a charging voltage of 4 kV, corresponding to electrical energy of 1.546 kJ charged to the capacitors.

Figure 2 shows the main electrical parameters describing the discharge pulse. The "current" in the figure denotes i_1, and "voltage" is deduced from i_2 and R_2. The dissipated power and energy

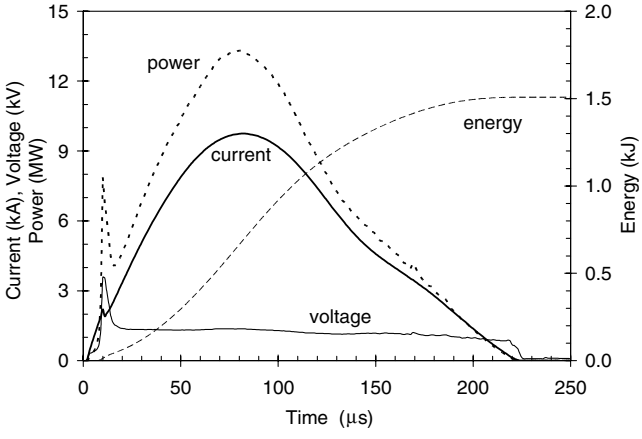

Fig. 2 Electrical parameters of capillary discharge.

deposited into the plasma were determined from the current (i_1) and the voltage.

Results of these parameters are quite consistent from test to test. The plots in the figure show that the 4 kV plasma pulse lasts about 225 μs and has a peak electric current of 9.75 kA appearing at 82 μs. The peak power was found to be about 13.31 MW at 81 μs. The sharp spikes appearing on the power and voltage traces at $\sim$10 μs indicate the completion of explosion of the wire and the formation of the initial plasma, which enables electrical conductance of the circuit to continue. A small change of slope in the current profile occurs at this time due to the shift of conducting medium from the metallic wire to charged particles in the plasma. As the discharge proceeds, more energy from the capacitors continues to deposit into the plasma in the capillary causing ablation of the capillary wall material (including the end electrode). Vaporization and ionization of the ablated material then yields much more plasma, which flows out the nozzle at high temperatures and pressures. As shown in the figure, most of the energy initially stored in the capacitors (1.536 kJ) is deposited into the plasma (1.507 kJ) and only a small portion ($\sim$1.86%) is consumed in resistive losses and/or remains in the capacitor as residue.

Plasma Impingement

When the plasma jet hits a flat plate that is perpendicular to the flow, the resulting surface pressure (stagnation pressure) is of great importance to understanding the impact of plasma jets on a propellant attached to the plate or a sample holder. Information about the surface pressure can help develop an understanding of possible mechanical effects on the propellant fracture before the occurrence of ignition. The jet structures exhibited during its evolution and interaction with the plate are an aid in such an understanding. To this end, both pressure data and jet structures were obtained from each test.

As the discharge begins, high pressures are rapidly built up in the capillary; consequently, the generated plasma is expelled out of the capillary through the nozzle, and then expands freely into the ambient air. After emerging from the capillary, the plasma flow evolves in a highly transient process. To temporally resolve these transients, the CCD camera was adjusted to have sufficiently short timings for both interframe (15 μs) and exposure (0.02 μs).

Figure 3 shows a series of CCD images representing a typical flow pattern of the plasma jet. For illustration purposes, the experimental setup was schematically shown in the last frame. In this test, the impinging distance or the plate location, denoted by $L_{n\text{-}p}$, is 40 mm. The initial efflux of plasma from the capillary causes a precursor shock, also known as a blast wave, to propagate into the ambient gas, which can be seen in Schilieren images [22], but not in the emission images presented here. This shock is almost spherical and expands radially as the transient proceeds. The early expansion of the plasma is primarily dominated by this spherical shock wave [23]. At about 75 μs, the jet approaches a quasisteady state and exhibits a structure, which, clearly, is characteristic of a highly underexpanded jet containing a shock cell featured by a barrel-shaped oblique shock and a slightly curved normal shock (Mach disk) [24,25]. This flow pattern has been found to be extremely complex, and a more detailed discussion can be found in a previous work [19].

Two regions of greatest luminosity are found in the images, one near the exit port and the other downstream of the Mach disk and against the plate. These brightest regions correspond to the highest temperature zones, as being confirmed by CFD modeling results [26].

As the jet impinges on the plate, the axial flow is halted and a stagnation region is formed. The jet is redirected and a flow in the radial direction is produced along the plate. The presence of the plate complicates the plasma jet flow due to interactions between shock waves in the jet and those created by the plate reflection. The shock interactions cause oscillations in surface pressures, as will be seen in the pressure data.

Figure 4 presents a typical result of the surface pressures at five locations of p_0, p_1, p_2, p_3, and p_4 resulting from impingement of the plasma jet on the plate at $L_{n\text{-}p} = 40$ mm. The pressure data in the figure give information about the times when the precursor shock arrives at each location, information on peak pressures, and oscillation of pressure. This oscillation behavior is also revealed in the diode signal at the jet front location, as shown in Fig. 5. The diode signal (D_2) indicates that the plasma jet front moves back and forth in the near wall region as a result of complex shock waves interaction and motions in the flowfield. The signal from diode D_1 shows that the plasma starts to emerge from the exit port at about 19 μs, and reaches the plate around 50 μs as indicated by the signal of D_2, corresponding to a speed of 1290 m/s. In addition, as shown by D_1, the emission luminosity of the plasma in the exit port region or the expansion fan reaches a maximum point at 67 μs, which is earlier than the times when the discharge reaches the peak power (81 μs) or the peak current (82 μs).

Of primary concern is how a propellant would behave when subject to such a plasma impingement. Therefore, studies were conducted with a double-based propellant, JA2, using the pressure transducers as well as the CCD imaging system. In actual ETC applications, the impinging distance, measured in $L_{n\text{-}p}$ or $L_{n\text{-}s}$, would be much smaller than 40 mm. Therefore, experiments were conducted over a range of $L_{n\text{-}p}$ or $L_{n\text{-}s}$ values down to 3 mm. The data will be discussed in two sets: distances of 40, 20, and 10 mm and distances of 8, 5, and 3 mm.

Figure 6 presents the centerline pressure data for 40, 20, and 10 mm. It can be seen from the figure, as the plate was moved closer to the nozzle exit, that dramatic changes in surface pressure are observed. The first change, which is not surprising, is the earlier

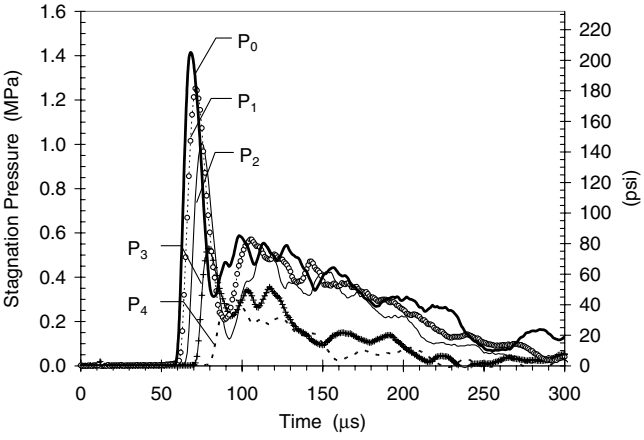

Fig. 4 Distribution of surface pressures along the stagnation plate. Pressure transducers are evenly spaced with P_0 at centerline ($L_{n\text{-}p} = 40$ mm).

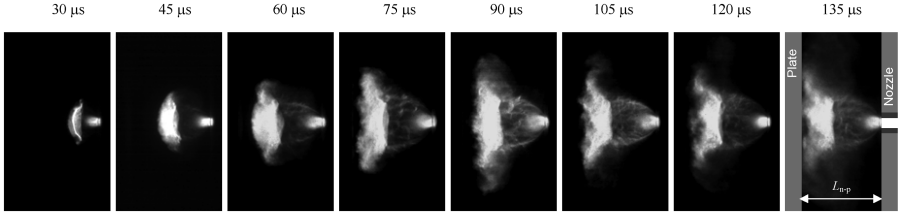

Fig. 3 Dynamic structures of a plasma jet showing features of an underexpanded supersonic jet ($L_{n\text{-}p} = 40$ mm).

arrival of the precursor shock as indicated by a sudden rise in the curves. The second change is observed in the oscillatory behavior of the pressure trace. These oscillations are very clear for the cases of $L_{n\text{-}p} = 40$ mm and $L_{n\text{-}p} = 20$ mm, but almost gone when $L_{n\text{-}p}$ is reduced to 10 mm. Moreover, at $L_{n\text{-}p} = 40$ mm, the surface pressure reaches a peak value of 1.40 MPa around 70 μs and then drops to several much smaller peaks less than 0.6 MPa; the drop is significant (about 57%). While at $L_{n\text{-}p} = 20$ mm, although the surface pressure varies similarly to the test at $L_{n\text{-}p} = 40$ mm, the drop from its highest peak (1.61 MPa) to smaller ones (as high as 1.25 MPa) is not significant (about 22%). The third change is the increase in the pressure. This increase is not very pronounced as $L_{n\text{-}p}$ is decreased from 40 to 20 mm, but is dramatic when $L_{n\text{-}p}$ is reduced to 10 mm. Some of these changes are also reflected in the diode signals shown in Fig. 7, where only diode signals near the impingement (D_2) are presented for these tests.

Pressure measurements for even closer impingement at $L_{n\text{-}p} = 8$, 5, and 3 mm were done also using the stagnation plate. Figure 8 presents the centerline surface pressure (P_0) from these measurements. For comparison, the pressure curve from the test at $L_{n\text{-}p} = 10$ mm is also plotted in the figure. The comparison shows a strong dependence of the pressure on the impinging distance. Experiments were also done to further reduce the value of $L_{n\text{-}p}$ to 1 mm; however, this proved to be an extremely harsh condition for

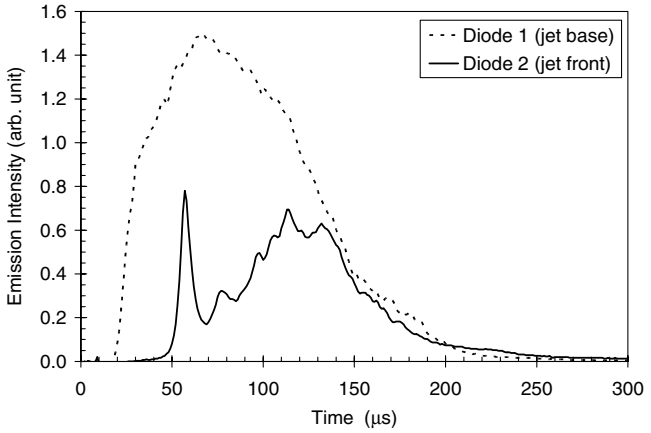

Fig. 5 Plasma emission intensities sensed by photodiodes at jet base and jet front ($L_{n\text{-}p} = 40$ mm).

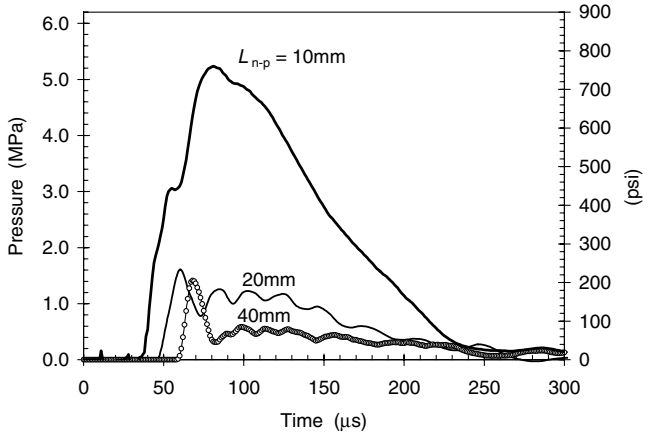

Fig. 6 Comparison of centerline surface pressure (P_0) at different impinging distances.

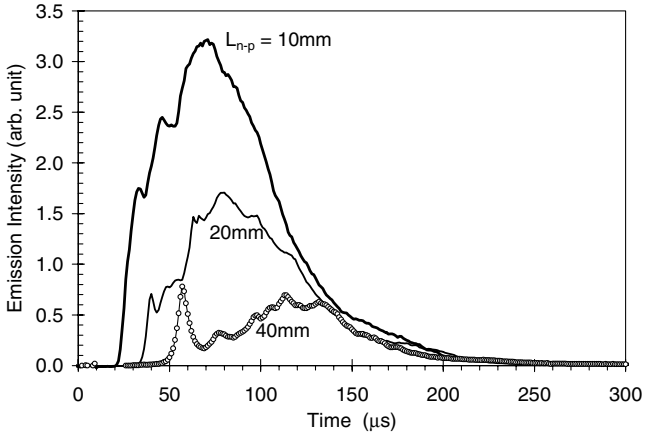

Fig. 7 Comparison of the diode signal for jet front emission (D_2) at different impinging distances.

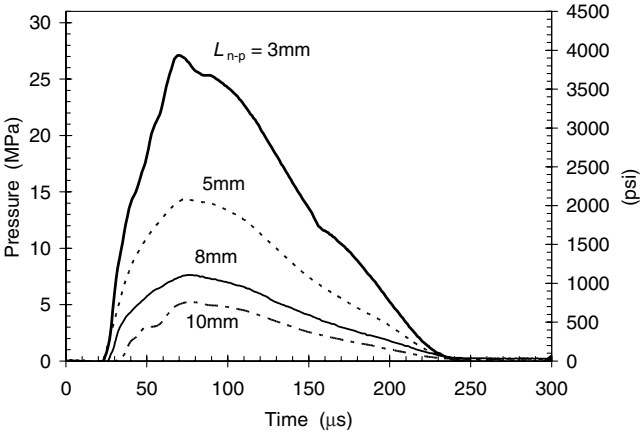

Fig. 8 Centerline surface pressure (P_0) at short impinging distances.

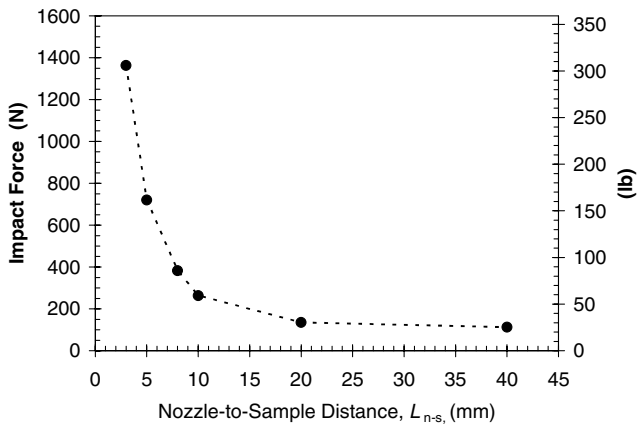

a)

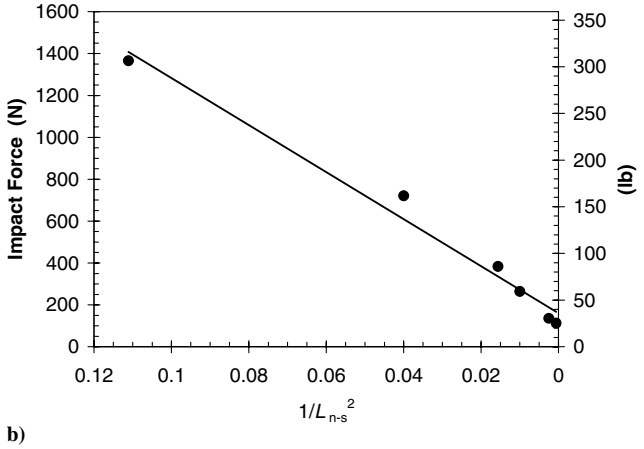

b)

Fig. 9 Impact forces on JA2 sample (10.5 mm in diameter) plotted as a function of a) impinging distances, $L_{n\text{-}s}$, and b) $1/L_{n\text{-}s}^2$.

the pressure transducer, because the insulation tape (even with two layers) that was used to protect the pressure transducer was torn up and burned during the impingement, resulting in failure of the pressure transducer. Nevertheless, it is obvious that the surface pressure will continue to increase and approach the pressure inside the capillary as the stagnation plate is moved closer and closer to the capillary exit port.

The impact force on a propellant when placed at the position of P_0 is of interest. This can be determined by knowing the size of the impinging area, which was found to depend on the nozzle-to-sample distance, $L_{n\text{-}s}$.

The curve in Fig. 9a shows the maximum impact forces that a JA2 sample (10.5 mm in diameter) would receive at different $L_{n\text{-}s}$. For the JA2 sample used in this work, the impinging area was measured to be $\sim$8 mm in diameter at $L_{n\text{-}s} \leq 10$ mm, but greater than the sample entire surface area at $L_{n\text{-}s} = 20$ mm and larger. Clearly, the critical effect of the impinging distance becomes increasingly important as this distance is getting smaller, as illustrated in Fig. 9b, which indicates that the impact force is inversely proportional to the square of $L_{n\text{-}s}$. When subject to such impingements at short distances, the sample is likely to fracture, which is especially true for thinner samples [19]. This fact suggests that, if the mechanical impact plays a role in ETC gun performance enhancement, the design of the plasma ignitor should place the propellant charge as close as possible to the plasma exit port.

The photographic studies using the CCD imaging system were also conducted during the impingement tests discussed above. Figure 10 shows typical images from tests with $L_{n\text{-}p}$ at 40 and 20 mm, and an image from tests with JA2 sample at $L_{n\text{-}s} = 5$ mm. Again, for illustration purposes, the experimental setups are shown in the figure

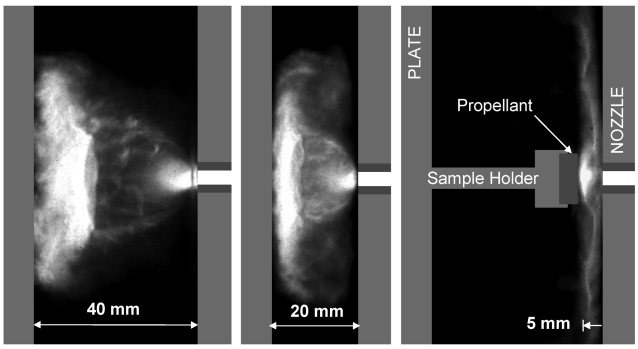

Fig. 10 Comparison of plasma jet structure at different impinging distances.

for each case. It is worth mentioning that these three images were all taken at $t = 105$ μs using the same exposure of 0.02 μs and f stop number (aperture) of 11.

It can be seen that decreasing $L_{n\text{-}p}$ from 40 to 20 mm brings about changes in the jet size, but the underexpanded jet structure still remains clear. Further reducing the impinging distance to 5 mm produces striking changes in the shock shapes. The distinct shock cell that is present in the left and middle images is replaced by a "swan-shaped" shock wave [19], which is developing in a narrow space defined by the nozzle exit plane and the sample surface plane. Quite interestingly, this shock structure acts as if the stagnation plate, rather than the JA2 sample whose surface area is much smaller than the plate, existed and confined the plasma within a 5 mm thick region. This unique feature is also seen in the images from tests with $L_{n\text{-}s}$ at 8 and 3 mm, as shown in Fig. 11, which also includes a full series of images for the case of $L_{n\text{-}s}$ at 5 mm.

The impingements at these short distances place the propellant sample under extreme conditions of high-pressure and high-temperature interactions with the plasma. These conditions caused considerable mass losses and significant surface modifications of the propellant, as will be seen in the following sections, but did not enable ignition or self-sustained combustion of the propellant sample due to the lack of confinement [18,19]. However, although no luminosity that would indicate ignition was observed during the impingement, judged by the CCD images as shown in Fig. 12, it is possible that ignition of the lost mass of JA2 was achieved and the lack of evidence is simply resulting from the combustion luminosity being overwhelmed by the extremely bright plasma [18].

Plasma-Induced Surface Phenomena of Propellant

The propellant sample has a disk shape cut from cylindrical sticks of standard JA2 (7-perf). Examination of the samples after impingement indicates changes in color and surface morphology. The color change is from dark green to yellow green occurring in a layer from the exposed surface down to about 1–1.5 mm. Blisters are observed along the side surface of this layer. A roughly pitted area about 6–8 mm in diameter that was recessed about 0.5–1.0 mm from the original surface is seen in the directly exposed region.

A detailed morphological analysis of this significantly modified surface was conducted using SEM coupled with x-ray detection for examination of any elemental variation. Figure 13 presents SEM microscopic images of the affected area with different magnification from 2.0 mm down to 20 μm; for comparison, an image of the virgin sample is also included in the figure. The SEM images show that, compared to the virgin sample, the exposed sample has dramatic changes in its surface morphology. Deformation of the perforations

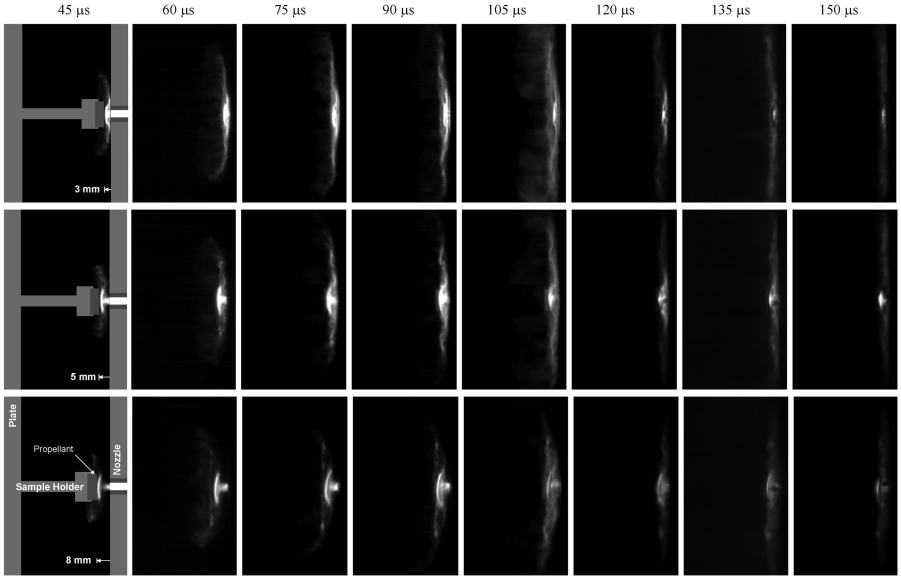

Fig. 11 Images of the plasma jet impinging on a JA2 sample at small impinging distances.

was found to be pronounced also. Evidences of melting, blisters as well as pits were observed on the surface through a closer look at the images with higher magnification.

The SEM images also show deposition of metallic particles on the affected area of the sample. As one can see from the images of the exposed JA2 in Fig. 13, there are some white particles sporadically distributed on the surface. And it should be noted that the actual color of these particles may not be white as it appears in the images.

Although the plasma is sustained by ablation of the capillary wall material, for the plasma generator used in this work, the total mass in the plasma jet is composed of contributions from several sources, including the end electrode (anode), trigger wire, nozzle (cathode), capillary, and the air that is initially in the capillary. Since the nozzle undergoes intense radiative and convective heating by the hot plasma flowing through it at high velocities, ablation of the nozzle surface material provides a major fraction to the total plasma mass. As a result, although by mole fraction the species from the hydrocarbon capillary dominate (about 90%) all other species, by mass fraction, it is the metals whose mass dominates the total mass of the plasma jet, as shown in Fig. 14. Therefore, it is not surprising that these metallic particles are present on the sample surface. The SEM images also show a broad size range of these particles, from one-tenth of a micron up to 50 microns.

These particles and their surrounding area were examined using an x-ray detector, the EDS, to identify the elemental compositions involved, and the results are shown in Fig. 15. The spectrum of a virgin JA2 sample (Fig. 15a) shows the relative intensities of the elements contained in the propellant. The lack of hydrogen (H) in the spectrum is due to the fact that the smallest atomic element that the EDS can detect is carbon (C). The results for the exposed JA2 sample are given in Figs. 15b and 15c, where the spectra were obtained from scanning over two large particles and a small circular region surrounding the particle. It was found that one particle contains copper (Cu) and tungsten (W), while the other only tungsten. It is noted that particles that contain only copper were also detected. The elements of carbon, nitrogen (N), and oxygen (O) are from the surrounding area. Figure 15d shows the spectrum scanning over a small area within which no clear evidence of particles is seen on the surface; however, tungsten can still be detected. This may suggest possible penetration of particles into the sample given the fact that in-depth detection of the x ray can be a few microns. It is also possible

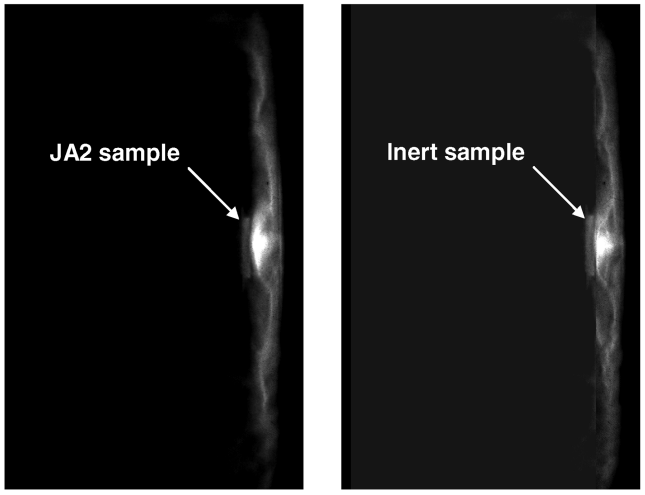

Fig. 12 Images of plasma impingement on the JA2 sample (left) and the inert sample (right) ($L_{n\text{-}p} = 5$ mm) showing no evidence of ignition with JA2.

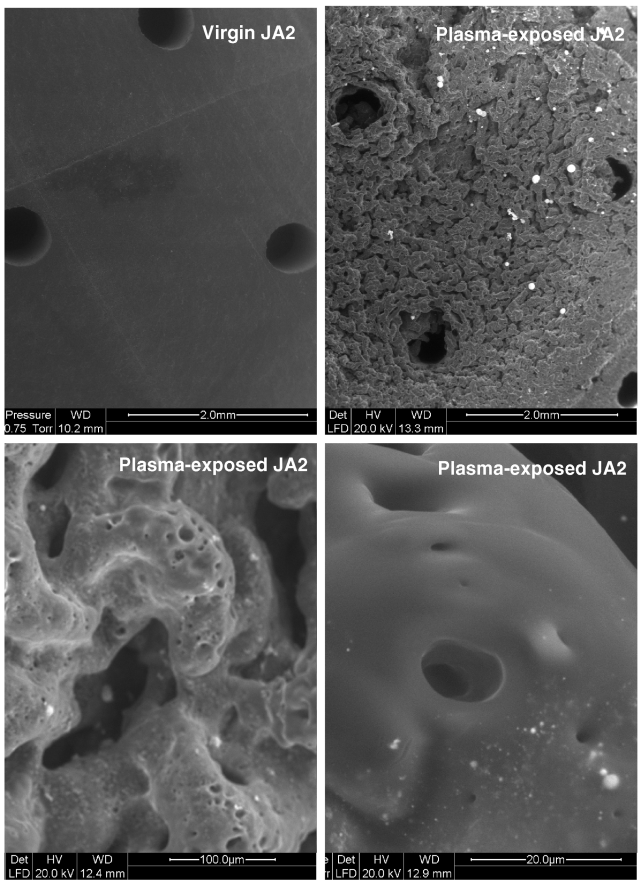

Fig. 13 Microscopic images of virgin and plasma-exposed propellant samples.

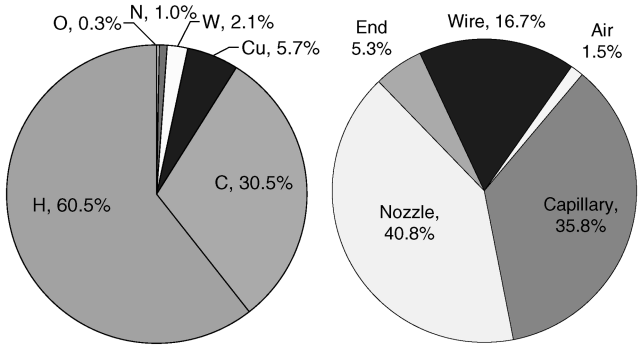

Fig. 14 Constituents of the capillary plasma: (left) by elemental composition, (right) by mass sources.

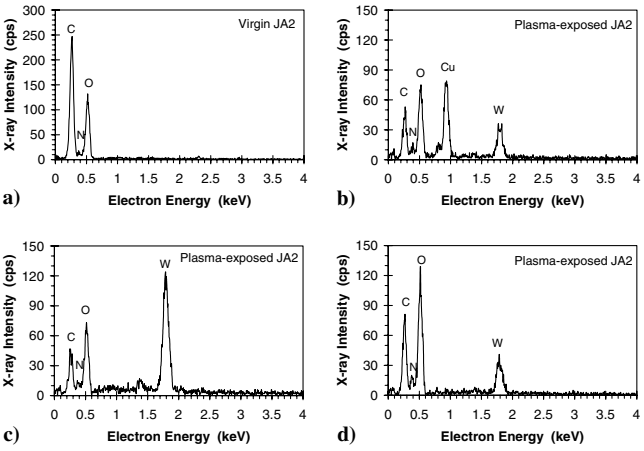

Fig. 15 X-ray spectra of virgin and plasma-exposed propellant sample: a) virgin sample; b) over a large particle on the exposed sample; c) over a different large particle; d) over a small affected area.

that a very thin film of the metal particles is formed on this area of the surface by a process similar to chemical vapor deposition.

It is worth mentioning that the copper more likely exists in oxides, but unfortunately the device cannot tell the oxidation status of metals. Taylor's work [16] indicates that oxidized copper residues are found on the surface of inert samples.

Another interesting finding is that, compared to the spectrum of the virgin JA2, the spectra of the exposed sample seem to suggest that the sample has lost more carbon, because the intensity of carbon was significantly decreased. This result seems to suggest that species containing carbon may be the major decomposed products leaving the propellant sample during the plasma interaction.

Mass Loss and Decomposition of Propellant

These observed surface phenomena are a strong indicator that in-depth heating causes decomposition of the propellant. Some of the gaseous decomposition products accumulated in bubbles that burst, leaving pits in the surface; others remained trapped inside the propellant resulting in internal bubbles and/or blisters. The surface modification also suggests erosive ablation of surface material due to intense heating and dynamic interaction by the plasma jet. This intense heating primarily results from radiative and convective heat transfer as well as from shock impingement heating. In-depth gasification and surface ablation result in mass loss of the propellant sample. This mass loss is strongly dependent on the impinging distance $L_{n\text{-}s}$ for a given charging voltage of the plasma.

As an example, Fig. 16 presents results from impingement tests at small $L_{n\text{-}s}$ values of 3, 5, and 8 mm. It can be seen that the amount of mass loss is quite repeatable for each case; the averaged mass loss is represented by the bar height. The actual amount of mass loss would be somewhat larger than the values in the figure, if the mass of metallic particles left on the sample were excluded.

An analysis of plasma-induced decomposition products of JA2 was conducted with a triple quadrupole mass spectrometer using electron impact ionization at 22 eV. The short time duration (less than 0.5 ms) of the open-air plasma does not match the TQMS response. Direct species measurement in closed-chamber configuration is desired, but the harsh conditions in the closed chamber would not allow the sampling probe to survive. These difficulties were overcome to some extent by using a plasma-holding chamber, which is a long (130 mm) cylindrical chamber with one end attached to the plasma generator and the other extending to a test chamber. A sample of JA2 was placed inside the chamber and brought close to the plasma exit port by a sample holder. A tubular sleeve of PE was inserted in the holding chamber to reduce the heat transfer from the plasma to the chamber walls, and to control the chamber actual volume to avoid ignition of the JA2 sample. On the bottom wall of the holding chamber, a second nozzle was installed that has a smaller orifice (1.0 mm) to slow down the flow out of the chamber. The jet from the holding chamber, called the secondary jet, has a substantially extended duration of typically around 50 ms, which is sufficiently long to match the timing requirement by the mass spectrometer. A sampling microprobe was placed 15 mm behind the second nozzle orifice, as seen in Fig. 17, which presents two images showing the microprobe submerged in the secondary jet for sampling species. It is seen from the images, the secondary jet in early times still exhibits a shock cell structure similar to the primary jet, but this feature soon disappears within a few milliseconds.

The species measurements were conducted at 4 kV and the holding chamber volume was adjusted to 45 cm^3 for both cases of with and without JA2 in the chamber. The test with JA2 has an $L_{n\text{-}s}$ at 5 mm. No ignition of the propellant was achieved, and the mass loss was similar to that in the open-air tests. Figures 18a and 18b compare the results from these species measurements. The normalized abundance in Fig. 18b was determined against the total ion counts (TIC). The number on the top of each bar represents the mass-to-charge ratio (m/z) for each detected ion, and the proposed species are listed in Table 1. Differentiation of species that have the same m/z

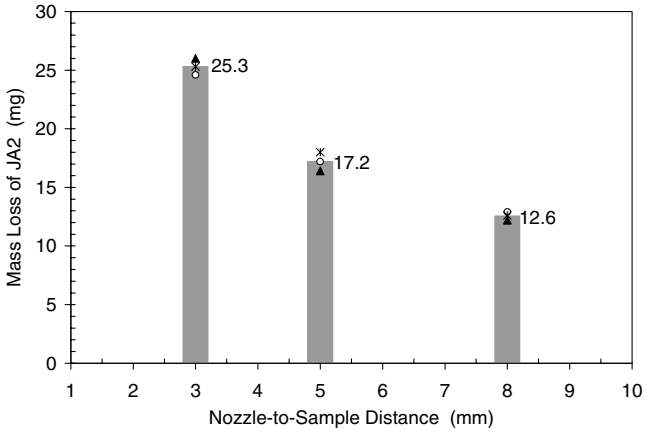

Fig. 16 Plasma-induced mass losses of 7-perf JA2 samples.

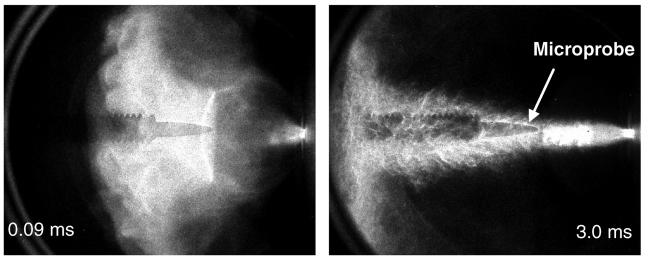

Fig. 17 Images showing a microprobe sampling of the jet discharging from the plasma-holding chamber.

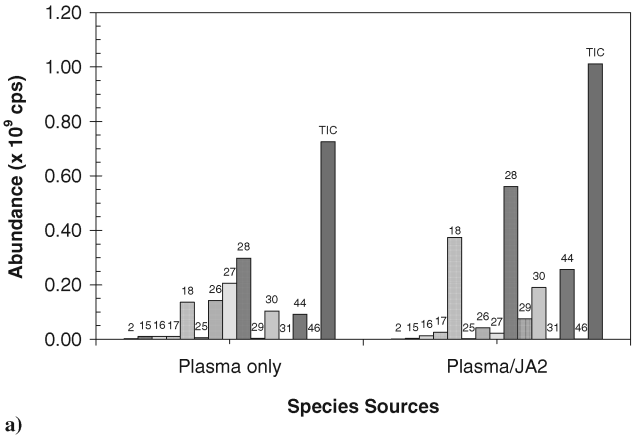

a)

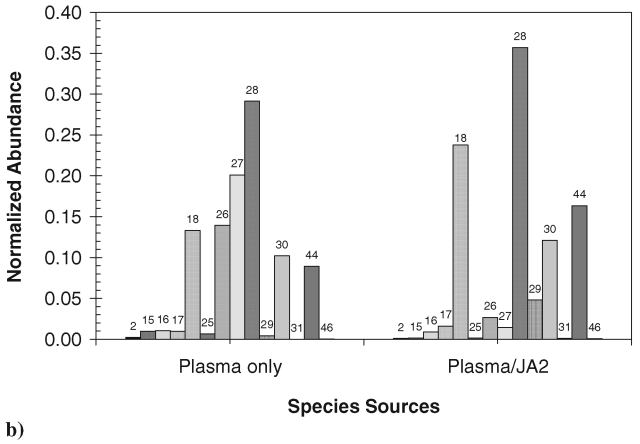

b)

Fig. 18 Comparison of species from plasma recombination and from plasma/JA2 interaction (the holding chamber is in 1 atm ambient condition before triggering the plasma) a) abundance in absolute values; b) normalized abundance over total ion counts.

Table 1 Detected species from recombined PE plasma and plasma/JA2 interaction

	Plasma only	Plasma and JA2	
m/z	Probable species	Probable species	Note
2	H_2	H_2	——
15	CH_3	CH_3	Fragment of CH_4
16	CH_4	CH_4	——
17	OH	OH	Fragment of H_2O
18	H_2O	H_2O	Increased with JA2
25	C_2H	C_2H	Fragment of C_2H_2
26	C_2H_2	C_2H_2	——
27	C_2H_3	C_2H_3	——
28	CO, C_2H_4	CO, C_2H_4	Increased with JA2
29	HCO	HCO	Increased with JA2
30	H_2CO, NO	H_2CO, NO	Increased with JA2
31	n/a	HNO	From JA2
44	CO_2	CO_2	Increased with JA2
46	n/a	NO_2	From JA2

Table 2 Species evolving from combustion of JA2 [27]

Reaction zone	Major combustion products
Fizz zone (surface)	NO_2
Dark zone	NO, H_2CO, CO, CO_2, H_2O, H_2
Flame zone	N_2, CO, CO_2, H_2O, H_2

value was enabled through an analysis of daughter ions using MS/MS methods.

In the test with plasma only, large amounts of species at m/z of 28, 27, 26, 18, 30, and 44 are usually observed, along with smaller amounts of 17, 16, 15, 25, 2, and 29. Compared to the result with plasma only, two major differences were found in the test with JA2. One is the appearance (in small amounts though) of species at m/z of 31 and 46; the other is the varied distribution of the relative intensities among all the species. Species with m/z of 31 and 46 were identified to be HNO and NO_2, respectively, which are from the propellant. To assist the analysis, the species evolving from different reaction zones during combustion of JA2 are listed in Table 2. It is interesting that the near surface species, NO_2, in the combustion of JA2 was seen as a decomposition product of the JA2 sample and survived during the plasma interaction.

The increased intensities for species at m/z of 18 and 44 show that the interaction of plasma with JA2 produces H_2O and CO_2, suggesting that ignition and combustion of part of the JA2 sample (the ablated mass) were achieved, since H_2O and CO_2 are typical dark zone and final products from JA2 combustion. Likewise, the increase in m/z of 28 is due to the formation of CO from the decomposed JA2, because C_2H_4 is not found as a product from JA2.

The increased m/z 30 in the test with JA2 is due to the contribution of both NO and H_2CO from JA2 to the abundance of ions at m/z 30. The increase in NO is confirmed by the MS/MS analysis for the daughter of m/z at 16, which is exclusively from NO, not from H_2CO. The formation of H_2CO is indicated by the increased HCO (m/z 29), a fragment of H_2CO resulting from electron impact in the ionizer [28].

The change in the ratio of species C_2H_2 (m/z 26) to C_2H_3 (m/z 27) may suggest that the interaction of plasma with JA2 changes the pathway of recombination reactions of the plasma species; the significant drop in their intensities is likely due to the decrease in their absolute amounts of production, but their volume fractions will also be reduced by dilution with reaction products from JA2.

Beyer and Pesce-Rodriguez [13] used Fourier transform infrared spectroscopy to analyze JA2 decomposition products induced by plasma radiation only and also found the presence of CO_2 and CO, but no detectable oxides of nitrogen. In their other work [29,30], chemical analysis of NO levels in recovered JA2 samples using desorption-gas chromatography-mass spectroscopy indicated enhancement of NO formation down to a depth of 0.75 mm from the surface, and suggested that NO is an early product of decomposition of nitrate esters but is sufficiently stable to remain trapped inside the sample. The reason that more species were detected in this work is probably because of ignition of the ablated JA2 once this part of lost mass is entrained into the plasma jet.

Conclusion

To better understand the interaction of the electrothermal plasma with propellants, several diagnostics were used to investigate the impingement of a capillary plasma on a plate or a JA2 propellant sample. The impinging pressure, jet structure, propellant surface modification, and mass loss as well as decomposition products of the propellant were discussed. Based on the experimental results, the main findings are summarized as follows:

1) The plasma jet structure changes as a function of the impinging distance, $L_{n\text{-}p}$ or $L_{n\text{-}s}$. The jet structure and its shock system at small $L_{n\text{-}p}$ or $L_{n\text{-}s}$ (8 mm under conditions of the present work) are distinctly different from those at relatively large distances.

2) The impinging distance strongly affects the surface pressure. The surface pressure varies as $1/L_{n\text{-}s}^2$, indicating that mechanical forces are very strongly affected by the distance from the plasma exit.

3) The responses of the JA2 sample include modification in surface morphology and mass loss. Metallic particles were found in the impingement area of the propellant sample, which are found to include tungsten and copper from the plasma source. It is likely that oxides of these elements are present in these particles, but the oxidation status of these elements cannot be determined using the SEM-EDS technique.

4) The identified species from JA2 as a result of plasma impingement were found to include H_2O, CO_2, CO, H_2CO, NO, HNO, and NO_2; the appearance of these species suggests that the lost mass of JA2 due to ablation is ignited.

Acknowledgements

This work was performed under the sponsorship of the Army Research Office, Contracts DAAG55-98-1-0519 and DAAD19-03-1-0340. The support and encouragement of D. M. Mann are greatly appreciated. Also the authors wish to acknowledge J. Yu at Alliant Techsystems—Radford Army Ammunition Plant for the shipment of JA2 propellant.

References

[1] Koleczko, A., Ehrhardt, W., Kelzenberg, S., and Eisenreich, N., "Plasma Ignition and Combustion," *Propellants, Explosives, Pyrotechnics*, Vol. 26, No. 2, 2001, pp. 75–83.

[2] Birk, A., Del Guercio, M., Kinkennon, A., Kooker, D. E., and Kaste, P., "Interrupted-Burning Tests of Plasma-Ignited JA2 and M30 Grains in a Closed Chamber," *Propellants, Explosives, Pyrotechnics*, Vol. 25, No. 3, 2000, pp. 133–142.

[3] Beyer, R. A., "Small Scale Experiments in Plasma Propellant Interactions," *Proceedings of the 37th JANNAF Combustion Subcommittee Meeting*, CPIA Publ. 701, Vol. 1, 2000, pp. 137–144.

[4] Kohel, J. M., Su, L. K., Clemens, N. T., and Varghese, P. L., "Emission Spectroscopic Measurements and Analysis of a Pulsed Plasma Jet," *IEEE Transactions on Magnetics*, Vol. 35, No. 1, 1999, pp. 201–206.

[5] Edwards, C. M., Bourham, M. A., and Gilligan, J. G., "Experimental Studies of the Plasma-Propellant Interface for Electrothermal-Chemical Launchers," *IEEE Transactions on Magnetics*, Vol. 35, No. 1, 1999, pp. 404–409.

[6] Katulka, G. L., and Dyvik, J. A., "Experimental Results of Electrical Plasma Ignition in 120-mm Solid Propellant Tank Gun Firings," *Proceedings of the 33rd JANNAF Combustion Meeting*, CPIA Publ. 653, Vol. 3, 1996, pp. 103–110.

[7] Marinos, C., "ETC Ignition and Temperature Sensitivity," *Proceedings of the 32nd JANNAF Combustion Meeting*, CPIA Publ. 631, Vol. 3, 1995, pp. 109–118.

[8] Chaboki, A., Zelenak, S., and Isle, B., "Recent Advances in Electrothermal-Chemical Gun Propulsion at United Defense, L. P.," *IEEE Transactions on Magnetics*, Vol. 33, No. 1, 1997, pp. 284–288.

[9] Wren, G. P., and Oberle, W. F., "Influence of High Loading Density Charge Configurations on Performance of Electrothermal-Chemical (ETC) Guns," *IEEE Transactions on Magnetics*, Vol. 37, No. 1, 2001, pp. 211–215.

[10] Perelmutter, L., Sudai, M., Goldenberg, C., Kimhe, D., Zeevi, Z., Arie, S., Melnik, M., and Melnik, D., "Plasma Propagation and Ignition in the Chamber of a SPETC Gun," *IEEE Transactions on Magnetics*, Vol. 35, No. 1, 1999, pp. 213–217.

[11] Wren, G. P., Oberle, W. F., and Hosangadi, A., "Influence of Radiation on Grain Heating in ETC Closed Chambers," *IEEE Transactions on Magnetics*, Vol. 35, No. 1, 1999, pp. 234–239.

[12] Schroeder, M. A., Beyer, R. A., and Pesce-Rodriguez, R. A., "Scanning Electron Microscope Examination of JA2 Propellant Samples Exposed to Plasma Radiation," *IEEE Transactions on Magnetics*, Vol. 41, No. 1, 2005, pp. 350–354.

[13] Beyer, R. A., and Pesce-Rodriguez, R. A., "The Response of Propellants to Plasma Radiation," *IEEE Transactions on Magnetics*, Vol. 41, No. 1, 2005, pp. 344–349.

[14] Das, M., Thynell, S. T., Li, J.-Q., and Litzinger, T. A., "Transient Radiative Heat Transfer from a Plasma Produced by a Capillary Discharge," *AIAA Journal of Thermophysics and Heat Transfer* (to be published).

[15] Wren, G. P., Oberle, W. F., and Hosangadi, A., "Influence of Radiation on Grain Heating in ETC Closed Chambers," *IEEE Transactions on Magnetics*, Vol. 35, No. 1, 1999, pp. 234–239.

[16] Taylor, M. J., "Ignition of Propellant by Metallic Vapour Deposition for an ETC Gun System," *Propellants, Explosives, Pyrotechnics*, Vol. 26, No. 3, 2001, pp. 137–143.

[17] Taylor, M. J., "Evidence for the Hypothesis of Ignition of Propellants by Metallic Vapour Deposition," *Propellants, Explosives, Pyrotechnics*, Vol. 27, No. 6, 2002, pp. 327–335.

[18] Li, J.-Q., Litzinger, T. A., and Thynell, S. T., "Plasma Ignition and Combustion of JA2 Propellant," *AIAA Journal of Propulsion and Power*, Vol. 21, No. 1, 2005, pp. 44–53.

[19] Li, J.-Q., Litzinger, T. A., and Thynell, S. T., "Interactions of Capillary Plasma with Double-Base and Composite Propellants," *AIAA Journal of Propulsion and Power*, Vol. 20, No. 4, 2004, pp. 675–683.

[20] Li, J.-Q., "A Study of an Electrothermal Plasma and its Interaction with Propellants," Ph.D. Dissertation, Mechanical and Nuclear Engineering Department, Pennsylvania State University, University Park, PA, May 2004.

[21] Li, J.-Q., and Litzinger, T. A., "Thermal Decomposition of 1-H-4-Amino-1,2,4-Triazolium Nitrate," *Combustion and Flame* (to be published).

[22] Kim, J. U., Clemens, N. T., and Varghese, P. L., "Experimental Study of the Transient Underexpanded Jet Generated by Electrothermal Capillary Plasma," *Journal of Propulsion and Power*, Vol. 18, No. 6, 2002, pp. 1153–1160.

[23] Wilson, D. E., Kim, K., and Raja, L. L., "Theoretical Analysis of an External Pulsed Plasma Jet," *IEEE Transactions on Magnetics*, Vol. 35, No. 1, 1999 pp. 228–223.

[24] Powell, A., "The Sound-Producing Oscillations of Round Underexpanded Jets Impinging on Normal Plates," *Journal of Acoustical Society of America*, Vol. 83, No. 2, Feb. 1988, pp. 515–533.

[25] Donaldson, C. DuP., and Snedeker, R. S., "A Study of Free Jet Impingement. Part 1. Mean Properties of Free and Impinging Jets," *Journal of Fluid Mechanics*, Vol. 45, No. 2, 1971, pp. 281–319.

[26] Nusca, M. J., McQuaid, M. J., and Anderson, W. R., "Development and Validation of a Multi-Species Reacting Flow Model for the Plasma Jet Generated by an ETC Igniter," *Proceedings of the 37th JANNAF Combustion Subcommittee Meeting*, CPIA Publ. 701, Vol. 1, 2000, pp. 181–199.

[27] Fifer, R. A., "Chemistry of Nitrate Ester and Nitramine Propellants," *Fundamentals of Solid-Propellant Combustion*, edited by K. K. Kuo, and M. Summerfield, AIAA, New York, 1984, Chap. 4, pp. 177–237.

[28] Lee, Y. J., "A Study of the Chemical and Physical Processes Governing CO2 Laser-Induced Pyrolysis and Combustion of RDX, BAMO, and RDX/BAMO Pseudo-Propellants," Ph.D. Dissertation, Mechanical and Nuclear Engineering Department, Pennsylvania State University, University Park, PA, May 1996.

[29] Pesce-Rodriguez, R. A., Beyer, R. A., Kinkennon, A. E., Del Guercio, M., Kaste, P. J., and Newberry, J. E., "In-Depth Chemistry in Plasma-Exposed M30 and JA2 Gun Propellants," *Proceedings of the 37th JANNAF Combustion Subcommittee Meeting*, CPIA Publ. 701, Vol. 1, 2000, pp. 145–155.

[30] Beyer, R. A., and Pesce-Rodriguez, R. A., "Experiments to Define Plasma-Propellant Interactions," *IEEE Transactions on Magnetics*, Vol. 39, No. 1, 2003, pp. 207–211.

M. Brewster
Associate Editor